International Journal of Applied Glass Science 1 [3] 296–308 (2010)
DOI:10.1111/j.2041-1294.2010.00021.x

INTERNATIONAL JOURNAL OF
Applied Glass
SCIENCE

Nonlinear Properties of Chalcogenide Glass Fibers

Jas S. Sanghera,* Leslie B. Shaw, Paul Pureza, Vinh Q. Nguyen, Dan Gibson, Lynda Busse, and Ishwar D. Aggarwal

Naval Research Laboratory, Washington, DC 20375

Catalin M. Florea

GTEC Inc., Crofton, Maryland 21114

Frederic H. Kung

University Research Foundation, Greenbelt, Maryland 20770

We demonstrate that the chalcogenide glasses possess large nonlinearities that can enable compact Raman amplifiers as well as fiber lasers and amplifiers in the mid-IR. These high nonlinearities also allow efficient supercontinuum generation, which is useful for broadband sources in the near and mid-IR. These materials can also be poled to induce an effective $\chi^{(2)}$, opening up the potential of waveguide parametric amplifiers and sources. The Brillouin gain coefficients are relatively large and enable the demonstration of slow light in small core fibers. Results lead to a figure of merit that is about 140 times larger, or a theoretical gain about 45 times larger, than the best silica-based fiber configurations reported to date.

Introduction

Chalcogenide glasses are based on the chalcogen elements S, Se, and Te with the addition of other elements such as Ge, As, and Sb to form stable glasses.[1] Because of their large IR transparency, fibers fabricated from these glasses are ideal for transmission of IR light and several applications of chalcogenide fibers have been documented.[2] Also of interest is the high nonlinearity of these glass compositions. The high third-order ($\chi^{(3)}$) nonlinearities of chalcogenide glasses make them excellent candidates for applications such as all optical processing, Raman amplification, parametric amplification, and supercontinuum generation.

*sanghera@nrl.navy.mil

Glass Preparation

Chalcogenide glasses are melted directly in quartz ampoules using chemicals purified via distillation/sublimation.[3] Typical melt temperatures range from 600°C to 900°C, depending upon composition. The liquids are quenched and the glass rods annealed at temperatures around the appropriate softening temperatures. The optical fibers are obtained by the double crucible (DC) process.[4] The DC process enables adjustments to be made in the core/clad diameter ratio during fiber drawing by independent pressure control above each melt. Therefore, both multimode and single-mode fibers can be drawn with relatively few processing steps. Furthermore, the fiber drawing capacity for both As–S and As–Se fiber is very similar.

Fiber Properties

Figure 1 compares the losses routinely obtained for a couple of chalcogenide glasses along with some lower losses reported in the literature.[5,6] Depending upon composition, sulfide, selenide, and telluride-based fibers transmit between about 0.8–7, 1–10 , and 2–12 6 μm, respectively. Therefore, practical applications dictate the type of fiber to be used. As–S fibers loss routinely achieved is about 0.1–0.2 dB/m in fiber lengths of about 500 m. Losses for As–Se fibers typically range from 0.5 to 1 dB/m in the near IR around 1.5 μm. The laser power handling capability can vary significantly depending on the type of laser, whether it is continuous wave (cw) or pulsed, the laser wavelength, and on the fiber core diameter. We have observed $>1.6\,GW/cm^2$ peak power density transmission without damage for pulsed lasers in the 2–5 μm wavelength region, and 240 KW/cm^2 cw power density at a wavelength of 5 μm.

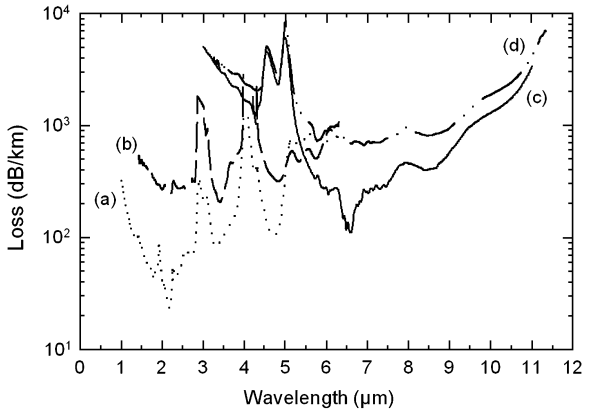

Fig. 1. Transmission loss spectra of (a) lowest loss sulfide fiber, (b) typical sulfide fiber, (c) lowest loss telluride fiber, and (d) typical telluride fiber.

Nonlinear Properties

It is well established that the values of $\chi^{(3)}$ for chalcogenide glasses are about two orders of magnitude larger than silica.[7,8] More recently, glasses have been reported with nonlinearities approaching 1000 times silica.[9,10] These large nonlinearities would allow small compact low power devices for telecommunications. The subpicosecond response of these nonlinearities is ideal for high data rate telecommunication devices.

For efficient nonlinear devices utilizing the optical Kerr effect, the nonlinearity must be high and the nonlinear absorption must be low. A figure of merit (FOM) $= n_2/(\beta\lambda)$ can be defined as a useful metric to determine optimum compositions, where n_2 is the nonlinear index and β is the nonlinear absorption. For isotropic medium, one and two photon resonant processes dominate the third-order susceptibility. For frequencies approximately half of the material resonance, two photon processes resonantly enhance the nonlinear index n_2. Normally, however, the two photon resonance enhancement is accompanied by two photon absorption (TPA), which competes with the nonlinear index n_2. In the case of amorphous materials such as chalcogenide glass, an exponential Urbach tail exists and its absorption edge extends below the half gap. This edge leads to TPA below the half gap and thus n_2 may increase faster than TPA absorption in this region. Consequently, the best performance in terms of nonlinear index strength versus TPA (as given by FOM) will occur just below the gap. Figure 2 shows the bandgap of the As–S–Se system versus Se concentration. Here, the bandgap is defined at the point of $10^3\,cm^{-1}$ absorption. In the graph, Se content of 0 at.% corresponds to pure As_2S_3 while Se content of 60 at.% corresponds to pure As_2Se_3. The bandgap of the glass system decreases with Se content. For operation at 1.55 μm (0.8 eV), we would expect an optimum composition of As_2Se_3 where $E_g/h\nu \sim 0.45$, which is borne out by experimental data.

Spectrally resolved two-beam coupling measurements of As–S–Se system have been performed to determine the magnitude of the nonlinear index n_2

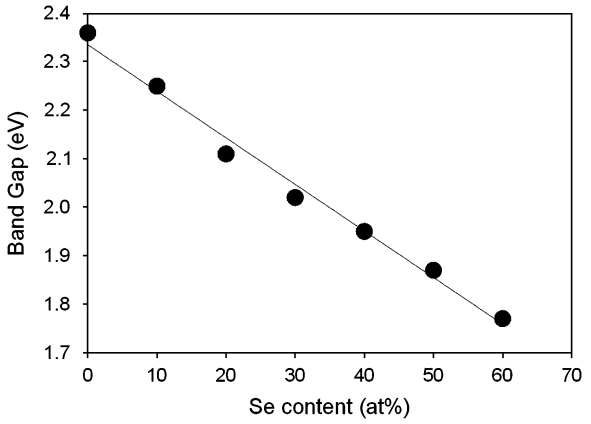

Fig. 2. Bandgap of As–S–Se glass system (defined at the point of 10^3 cm^{-1} absorption).

and the TPA coefficient. Details of these measurements can be found elsewhere.[10] Figure 3 shows the results of these measurements. Values for As–S were found to be ~220 times higher than for silica at 1.55 μm and increased with Se substitution of S to a value of ~930 times higher than silica for As–Se. Likewise, TPA also increases with an increasing Se content. These data can be used to calculate the FOM for the As–Se system (Fig. 4). As expected, the largest FOM for operation at 1550 nm occurs for the glass with $E_g/h\nu$ at ~0.45, which is the As–Se composition.[11]

High-speed optical processing has been demonstrated by exploiting these high nonlinearities in chalcogenide glass fiber and waveguides. Earlier work on all optical switching in chalcogenide fiber was performed by Asobe *et al.*[12] who demonstrated switching of an 80 GHz pulse train in a 2 m length of As_2S_3-based fiber

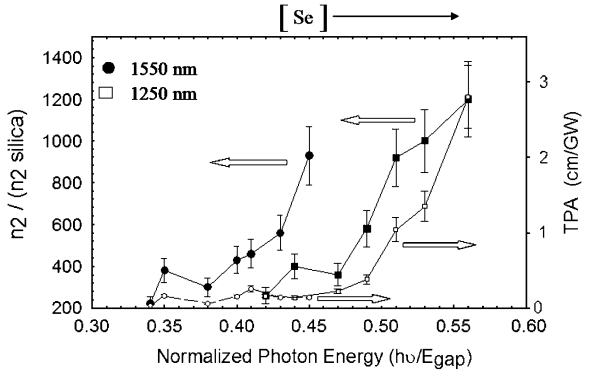

Fig. 3. n_2 and two photon absorption (TPA) absorption of As–S–Se glass system.

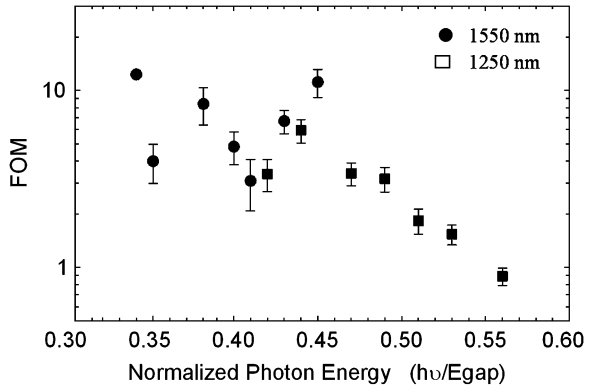

Fig. 4. Figure of merit (FOM) for As–S–Se glass system.

using an optical Kerr shutter configuration. More recently, 640 Gb/s demultiplexing has been demonstrated in a 5 cm long chalcogenide rib waveguide on silicon by utilizing FWM.[13] All 40 Gb s^{-1} optical wavelength conversion has also been demonstrated in chalcogenide tapered fibers.[14] Here, a cw laser at the conversion wavelength was modulated by XPM with the copropagating 40 Gb/s signal.

Raman Amplification

Figure 5 shows the normalized Raman spectra of As_2S_3, As_2Se_3, and silica. The As_2Se_3 glass has a much narrower Raman line (~60 cm^{-1}) than silica glass (~250 cm^{-1}). In addition, the Raman shift for $As_{40}Se_{60}$ glass is much smaller (~240 cm^{-1}) than the Raman shift of silica glass (~440 cm^{-1}) due to the heavier atoms present in the chalcogenide glass. Previous studies have looked at stimulated Raman scattering (SRS) in $As_{40}S_{60}$ glass, a very similar glass system to As_2Se_3.[15] These studies found the Raman gain coeffi-

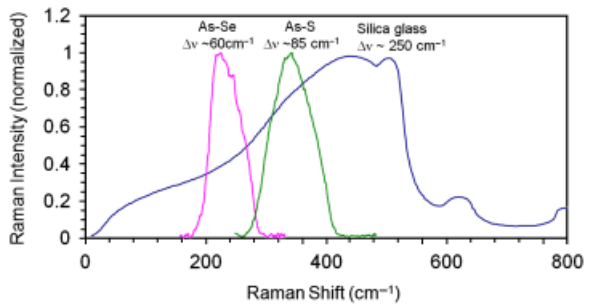

Fig. 5. Raman spectra of As_2S_3 and As_2Se_3 glass. Silica glass is shown for reference.

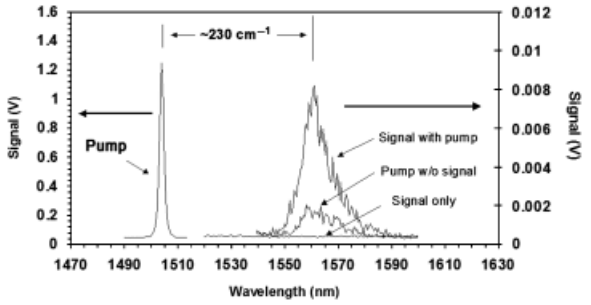

Fig. 6. Raman amplification in As–Se fiber. Shown is the amplifier output with signal and no pump, pump and no signal (showing background stimulated Raman scattering resulting from pump), and amplified signal with pump.

cient of $As_{40}S_{60}$ to be almost two orders of magnitude higher than that of silica. It was also found that this enhancement in the Raman gain roughly corresponded to the enhancement in the nonlinear index, n_2. Consequently, one might expect to see an even larger Raman gain coefficient in As_2Se_3 because the selenide glass has shown an even larger nonlinearity and also a narrower Raman spectrum.

Raman amplification at 1.55 μm has been demonstrated in small core As–Se fiber.[16] The results of the Raman amplification experiment are shown in shown in Fig. 6. Over ~23 dB of gain was achieved in a 1.1 m length of fiber pumped by a nanosecond pulse of ~10.8 W peak power at 1.50 μm. The peak of the Raman gain was shifted by ~230 cm^{-1} to 1.56 μm. The Raman gain coefficient was estimated to be ~300 times higher than for silica in this experiment. More recent measurements of the Raman gain coefficient show a value of about 780 times greater than that of silica.[11]

The large Raman gain coefficient of chalcogenide glass coupled with its large IR transparency show promise for lasers and amplifiers in the near and mid-IR. The potential for Raman lasers and amplifiers can be assessed by defining a FOM. The expression for single pass gain, G_A, in a Raman fiber laser is given below:

$$G_A = \exp\left(\frac{g_R P_0 L_{eff}}{A_{eff}}\right) \quad (1)$$

where g_R is the Raman gain coefficient, P_0 is the pump power, A_{eff} is the fiber effective area, and L_{eff} is the fiber effective length. The fiber effective length is given by

$$L_{eff} = \frac{1}{\alpha}(1 - e^{-\alpha L}) \quad (2)$$

where α is the fiber loss. For long lengths, L_{eff} is approximately $1/\alpha$. From these equations, the gain is proportional to $\exp(-g_R/\alpha)$ for long fiber lengths. Thus, the value g_R/α can be used as a rough FOM for Raman amplification. Table I compares the performance of an As–Se Raman fiber laser or amplifier operating at 4 μm to a silica Raman fiber laser or amplifier operating in the telecommunications band at 1.5 μm. Here, the Raman gain coefficient of As–Se, g_R, which is measured to be 780 times higher than silica at 1.5 μm is extrapolated to its value in the mid-IR because the Raman gain coefficient scales inversely with wavelength. For silica, a loss of 0.2–0.3 dB/km is typical of telecommunication-grade fiber. For As–Se, two losses are given. The loss of 200 dB/km is an example of a low loss achieved at NRL for As–Se fiber while the loss of 3 dB/km is the theoretical loss for As–Se fiber.[17] For the loss of 200 dB/km, the value of g_R/α for an As–Se fiber Raman amplifier operating at 4 μm is about 0.38 compared with 1.1 for a silica fiber Raman amplifier at 1.5 μm. Using the theoretical loss of 3 dB/km, the value of g_R/α for As–Se fiber at 4 μm is 23 times higher than for silica fiber operating at 1.5 μm.

A Raman laser has been demonstrated in As–Se.[18] The authors generated 0.64 W of first Stokes at 2062 nm with a slope efficiency of 66% under 2051 nm pumping in a 1 meter length of fiber (6 μm core, 0.19 numerical aperture (NA), 0.6 dB/m loss).

Table I. Figure of Merit for Raman Amplification in As–Se Fiber at 4 μm Compared with Raman Amplification in Silica Fiber at 1.5 μm

	λ (μm)	g_R (cm/W)	Loss (dB/km)	α (cm^{-1})	FOM ($10^{-6}W^{-1}$)
Silica fiber	1.5	0.65×10^{-12}	0.2–0.3	$\sim 0.6 \times 10^{-7}$	1.1
As–Se fiber	4	1.7×10^{-10}	200	5×10^{-4}	0.34
			3	7.5×10^{-6}	23

The loss values of 200 and 3 dB/km for As–Se are representative of a typical low loss fiber and the theoretical loss, respectively.
FOM, figure of merit.

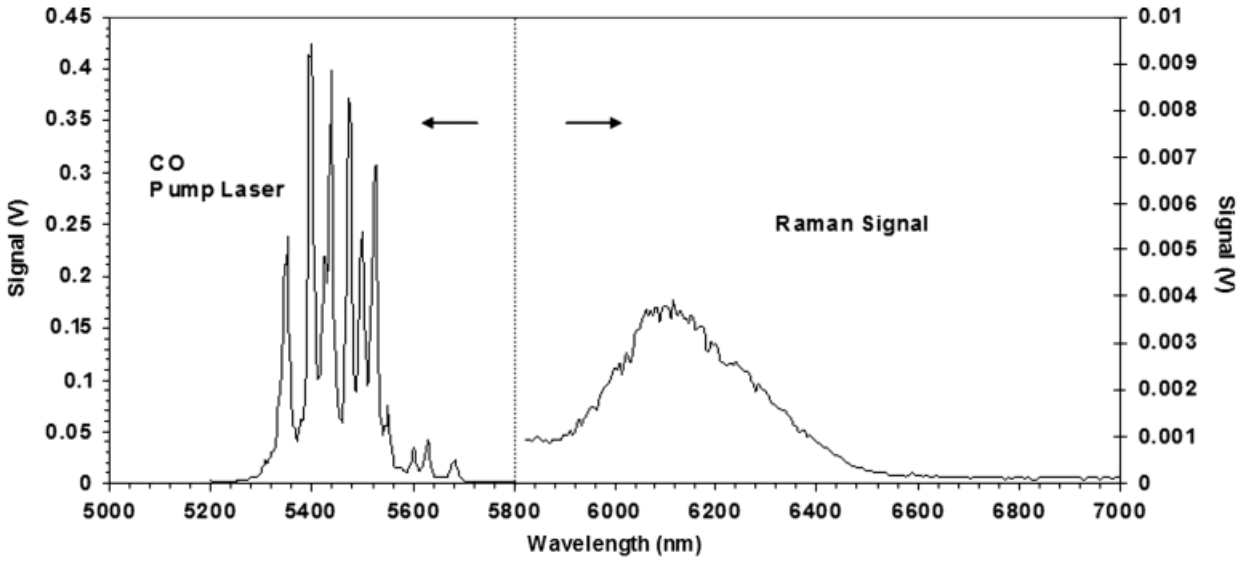

Fig. 7. Stimulated Raman scattering signal observed at 6.1 μm under ~5.4 μm CO laser pumping.

Reflection off the endface of the fiber (~22% at normal incidence) was used for feedback at the output end of the fiber while a broadband Au-coated mirror was used as a back reflector. Note that the broadband nature of the cavity reflectors allowed the Raman laser to oscillate on a number of vibrations. The line at 2062 nm was attributed to interlayer vibrations of As_2Se_3. Raman output at 2102 nm from bond bending vibrations and at 2166 nm for bond stretching vibrations were also observed.

SRS has been observed in the mid-IR. Figure 7 shows the SRS in a ~1 m length of As–Se fiber under cw CO laser pumping at ~5.4 μm. The SRS is seen at ~6.1 μm. Raman laser operating in the wavelength range from 6.1 to 6.4 μm would have applications in laser surgery. These wavelengths correspond to amide bands in tissues and studies have shown that ablation of soft tissue is possible at these wavelengths with minimal collateral damage, thus accelerating healing.[19] Modeling of a Raman laser operating at 6.45 μm under CO laser pumping at 5.59 μm has demonstrated high slope efficiencies and moderate threshold power for operation.[20]

Supercontinuum Generation

Supercontinuum generation has been demonstrated between 2 and 3 μm in small core sulfide and selenide fibers as well as photonic crystal selenide fibers (PCF).[21] The 1 m lengths of fiber were pumped with a Ti:sapphire pumped OPA laser at a wavelength of 2.5 μm using 100 fs pulses and 100 pJ/pulse. The outputs from the fibers are shown in Fig. 8. The sulfide and selenide fibers had 7 μm core diameter, while the PCF fiber had a 10 μm core diameter. In all cases, pumping was in the normal dispersion region of the fibers and much of the broadening can be attributed to self phase modulation with some broadening to the red due to Raman scattering.[22]

By using chalcogenide glass PCF, the dispersion of the fiber can be controlled and the zero dispersion wavelength can be shifted to the near-IR making it feasible to pump in the anomalous dispersion region of the fiber

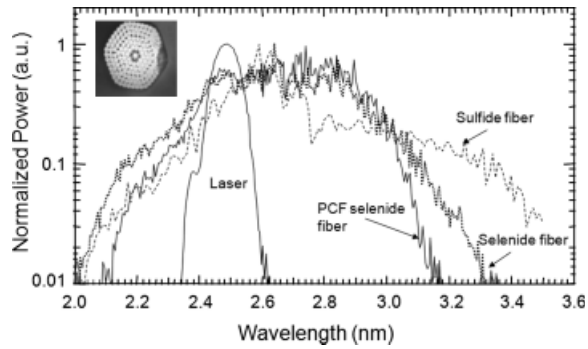

Fig. 8. Supercontinuum generation in small core chalcogenide fibers. The insert shows the cross-sectional view of the selenide photonic crystal fiber (PCF) fiber.

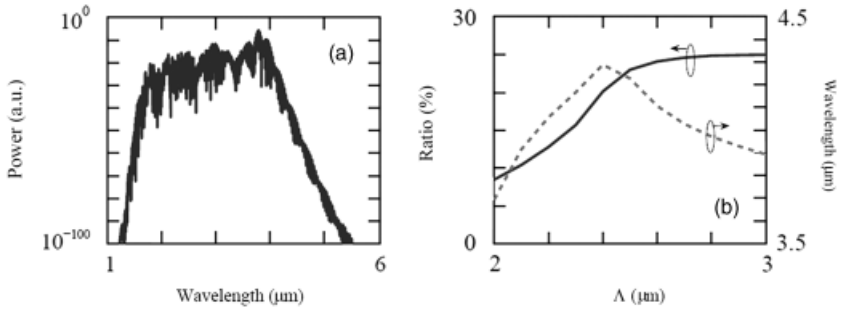

Fig. 9. (a) Modeled supercontinuum spectrum in As–S photonic crystal fiber (PCF) with Λ = 3 μm under 2 μm, 500 fs, 1 kW peak power pumping. (b) The central wavelength of the soliton with the largest power (dashed curve) and the ratio of the power generated between 3 and 5 μm to the total input power as a function of the pitch at the end of the tapered PCF (solid curve).[23]

with conventional near-IR fiber laser pumps. Modeling has shown that very broad supercontinuum bandwidths can be generated with properly designed chalcogenide PCF fiber and proper pump (Fig. 9).[23]

Poling of Chalcogenide Glass

Isotropic materials, such as glasses, lack a center of inversion symmetry and thus have no second-order nonlinear susceptibility ($\chi^{(2)}$) and they should not exhibit second harmonic generation (SHG).[24] However, undoped and Pr-doped GaLaS glasses have exhibited SHG through optical pumping.[25] This SHG may be due to crystallization or the effect of frozen-in electric fields. The latter arises from the relationship $\chi^{(2)} = E_{dc}\chi^{(3)}$, where E_{dc} is the frozen-in electric field.[24] Electric poling has been successfully used to produce SHG in silica-based fiber systems.[26] It is not unreasonable to expect similar results in chalcogenide fibers. Because $\chi^{(3)}$ is about two to three orders of magnitude larger in chalcogenides compared with silica, we expect larger SHG efficiencies in electrically poled chalcogenide glasses. However, the question arises as to whether the electric fields can be frozen-in for chalcogenide glasses. SHG has been observed at 780 nm using electrically poled arsenic sulfide glass when pumping a 1-mm-thick arsenic sulfide glass disk at 1560 nm as shown in Fig. 10. The sample was electrically poled at 100°C for 5 h under nitrogen gas atmosphere. At the present time, the magnitude appears comparable with silica glass but the mechanism is unknown. Albeit, the effect was still observed with similar magnitude after surface polishing, indicating this is most likely a bulk effect with negligible surface contribution.

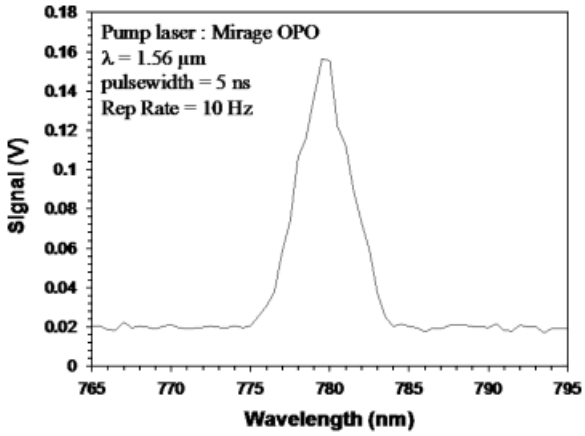

Fig. 10. Second harmonic generation at 780 nm in poled As–S glass pumped at 1.56 μm.

Brillouin Scattering

In order to estimate the Brillouin gain coefficient, the threshold power of the stimulated Brillouin scattering (SBS) process can be measured using the experimental setup detailed in Fig. 11. The threshold power is

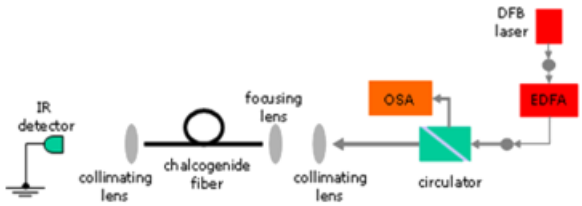

Fig. 11. Experimental setup used for stimulated Brillouin scattering threshold measurements. OSA, optical spectrum analyzer; IR, infrared; EDFA, Er-doped fiber amplifier; DFB, Distributed feedback.

easily determined by measuring the amount of power or by monitoring the spectrum of the reflected light, using a high-resolution optical spectrum analyzer (OSA) and a fiber circulator. The fibers are coated with liquid gallium on 10 cm lengths on each end to eliminate the radiation leaking into the cladding. In the example provided, the fiber ends were not antireflection coated and hence cavity effects were significant due to the high refractive index of the fiber. The losses in the fiber and in the coupling optics are all taken into account when estimating the amount of pump launched into the core. A 45% coupling efficiency was estimated in the As_2S_3 case, and 37% in the As_2Se_3 case. These values can be optimized and hence the SBS threshold power can be reduced, which is desired from a system design perspective. The spectral changes of the backward wave propagating through the chalcogenide fiber, as sampled by the circulator, are shown in Fig. 12 for the As_2S_3 fiber, and in Fig. 13 for the As_2Se_3 fiber, respectively. The cavity effects reduced the accuracy of the threshold measurement as indicated in the captions. Nevertheless, the threshold is easily identified by the significant jump in the peak of the Brillouin-shifted signal monitored on the OSA. Additionally, clamping of the pump output power was observed once the threshold was reached, as most of the pump power was transferred to the Stokes wave.[27]

The NA of a fiber determines the mode-field diameter (MFD) and hence the effective area of the fundamental mode, with direct implications on the threshold power estimation for the SBS process. It also determines the number of modes supported by the fiber at a given wavelength, λ. The *V*-number for a step-index fiber is a function of NA as given in the following equation, where *d* is the core diameter

$$V = \frac{\pi d}{\lambda} \mathrm{NA} \tag{3}$$

A value of $V = 2.405$, or lower, indicates single mode behavior. The *V*-number for the As_2S_3 fiber used was ~2.8. During the experiments, the mode field pattern was monitored by imaging the output on a Vidicon camera to make sure only the fundamental mode was launched. Using the NA and *V*-number values, the MFD, $d^2_{1/e}$, for the fundamental mode will be given by the following equation and is listed in Table II:

$$d_{1/e^2} = d \times \left(0.65 + \frac{1.619}{V^{1.5}} + \frac{2.879}{V^6}\right) \tag{4}$$

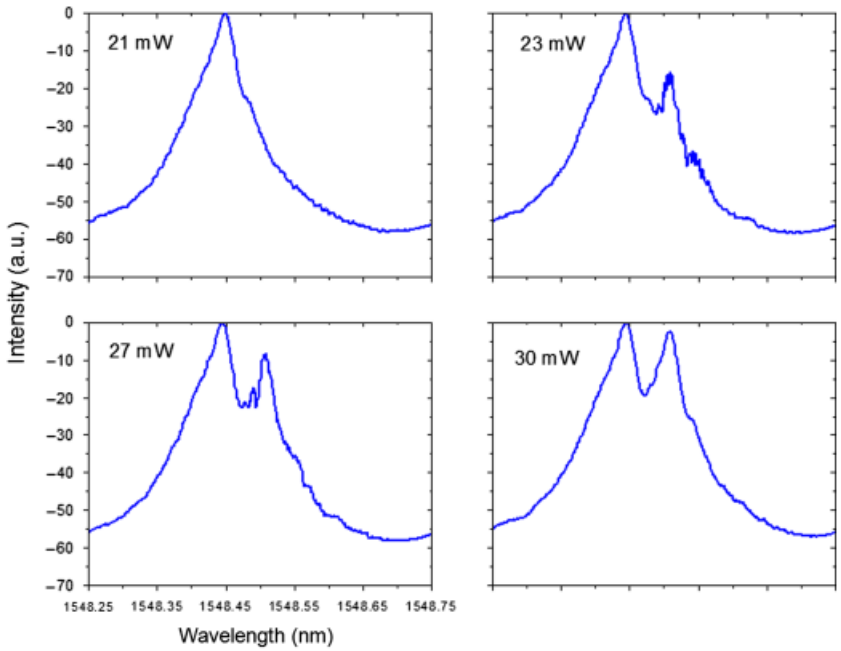

Fig. 12. Typical spectra of the reflected light sampled by the circulator for different launched pump powers into the As_2S_3 fiber core. Fiber length was 10.0 m. Estimated stimulated Brillouin scattering threshold: (27±3) mW. Tick labels shown only on one plot for clarity.

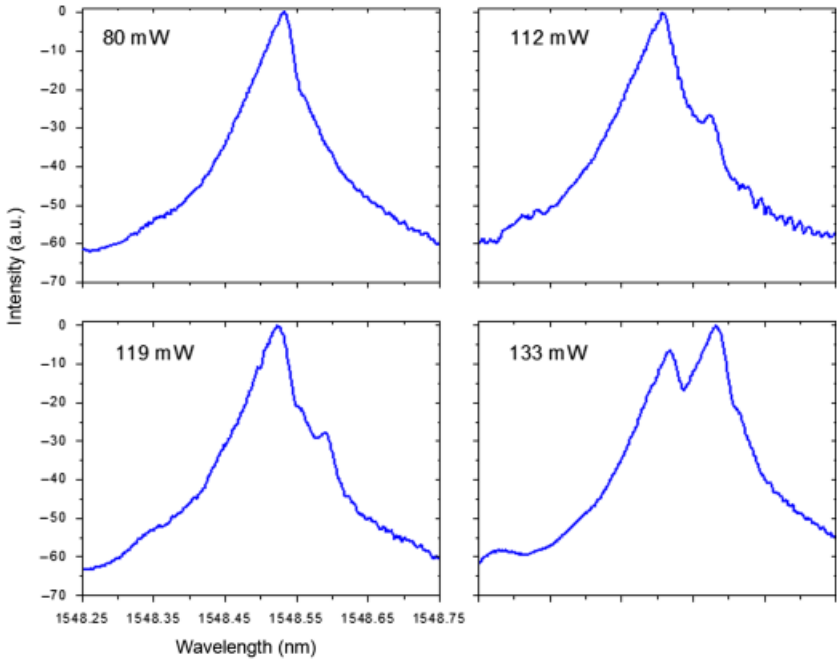

Fig. 13. Typical spectra of the reflected light sampled by the circulator for different launched pump powers into the As_2Se_3 fiber core. Fiber length was 5.0 m. Estimated stimulated Brillouin scattering threshold: (127±7) mW. Tick labels shown only on one plot for clarity.

The propagation loss is also an important parameter as it defines the effective interaction length for the Brillouin scattering process. The values reported in Table II represent relatively low losses for both single-mode fibers at 1.56 μm. However, it should be possible to lower the losses even further by improved fiber drawing and glass fabrication processes.

From the experimentally determined threshold power values (P_{th}) shown in Figs. 12 and 13, one can estimate the Brillouin gain coefficient (g_B) using the following equation:[28,29]

$$P_{th} \cong 21 \frac{A_{eff}}{L_{eff} g_B k} \tag{5}$$

In the Eq. (5), k is a constant that reflects whether the polarization is maintained constant throughout the interaction ($k = 1$) or not ($k = 0.5$, our case). Also, the A_{eff} and L_{eff} are the effective area of the fundamental mode, and the effective interaction length, respectively. These are given by Eqs. (6) and (7), where L is the fiber length, α is the propagation loss, and the MFD is determined by Eq. (3) above

$$A_{eff} = \frac{\pi d_{1/e^2}^2}{4} \tag{6}$$

$$L_{eff} = \frac{1}{\alpha}\left(1 - e^{-\alpha L}\right) \tag{7}$$

Using Eqs. (5)–(7), the parameters from Table III, and the fiber lengths and pump threshold values indicated in Figs. 11 and 12, the Brillouin coefficient is estimated to be $(3.9 \pm 0.4) \times 10^{-9}$ m/W for the As_2S_3 and $(6.75 \pm 0.35) \times 10^{-9}$ m/W for As_2Se_3. The value for the As_2Se_3 is close to the only other previously published

Table II. Chalcogenide Fiber Parameters at a Wavelength of 1.56 μm

Fiber	Core diameter (μm)	Clad diameter (μm)	Core refractive index	NA	V-number	$d_{1/e2}$ MFD (μm) (calculated)	Loss (dB/m)
As_2S_3	4.2	142.0	2.45	0.33	2.8	4.2	0.57
As_2Se_3	6.5	175.0	2.81	0.14	1.8	9.0	0.90

Table III. Comparison of Figure of Merit (FOM) for Slow-Light-Based Applications at 1.56 μm

	Silica[34,35]	Bi-HNL[31]	As_2Se_3[28]	As_2Se_3	As_2S_3
n	1.47	2.22	2.81	2.81	2.45
A_{eff} (m^2)	6.78×10^{-11}	0.3×10^{-11}	3.94×10^{-11}	6.31×10^{-11}	1.39×10^{-11}
loss (dB/m)	0.001	0.91	0.84	0.90	0.57
L (m)	2.0	2.0	5.0	5.0	10.0
L_{eff} (m)	2.0	1.63	3.23	3.1	5.6
g_B (m/W)	4.40×10^{-11}	6.43×10^{-11}	6.10×10^{-9}	6.75×10^{-9}	3.90×10^{-9}
G_{th} (dB)	0.076	0.003	1.084	0.719	3.398
FOM (dB/W/m)	1	17	77	51	139

result for this composition.[28] The value for the As_2S_3 fiber, although lower than the one for As_2Se_3, is still almost two orders of magnitude higher than that for fused silica ($\sim 4.4 \times 10^{-11}$ m/W).[28,30]

Slow Light

The slow-light technique based on SBS in optical fibers has attracted interest as it allows a very simple and robust implementation of tunable optical pulse delays, using mostly standard telecom components. Especially important are nonsilica-based fibers with higher nonlinearity because these require lower powers and shorter lengths for practical implementations.

To date, there have been reports of slow-light generation in bioxide high-nonlinearity fiber,[31] tellurite fiber[32] and of very efficient slow- and fast-light generation in As_2Se_3 chalcogenide fiber.[28] Additionally, the SBS process has been studied in As_2S_3 glass fibers.[33] The very large Brillouin gain coefficient presents the chalcogenide fibers as alternatives to silica fiber for slow-light applications. A FOM has been proposed in order to quantify the usefulness of a given fiber for slow-light-based applications.[28] The Brillouin gain is considered a positive factor while the length, the refractive index, and the power are considered as negative factors impacting the response time and the onset of additional nonlinear effects in the system. The FOM requires knowledge of the actual Brillouin gain that has to be measured, and takes into account the effective length and not the total length of fiber. One can rewrite the FOM such as to reduce it to the primary quantities describing the fiber (effective area, length and propagation loss, refractive index, and Brillouin gain coefficient expressed in dB):

$$\mathrm{FOM} \equiv \frac{\mathrm{Gain\,(dB)}}{P_p n L} = \frac{10 \times \log\left(\exp\left(g_B k \frac{P_p}{A_{eff}} L_{eff}\right)\right)}{P_p n L} \quad (8)$$

The FOM can be further reduced to

$$\mathrm{FOM} = 4.34 \frac{g_B k L_{eff}}{n A_{eff} L} \quad (9)$$

It is important to keep in mind that this FOM essentially determines what length and power are needed in a system to achieve a certain gain, and hence a certain time delay. The FOM as defined above in Eq. (9) tends to be a quantity that obscures the physical meaning contained in Eq. (8). Actually, the theoretical gain (G_{th}), expressed in dB, as given by Eq. (10), could be used instead to compare different fibers, if one considers a standard fiber length of 1 m and a standard pump power of 1 mW. Then, the theoretical gain is given by the following equation:

$$G_{th}[\mathrm{dB}] = 4.34 \frac{g_B k \times 1\,\mathrm{mW} \times L_{eff}|_{L=1\,m}}{A_{eff}} \quad (10)$$

One can use this last, fairly simple expression to compare the most representative fibers considered so far: silica,[34,35] high-nonlinearity bismuth fiber,[31,36] As_2Se_3 fiber,[28] along with the results reported here. The comparison is provided in Table III, with all the data reported for experiments without polarization control ($k = 0.5$). Also included is the FOM as defined above for completion. One can easily notice the significant increase in the theoretical gain (or FOM) for the As_2S_3

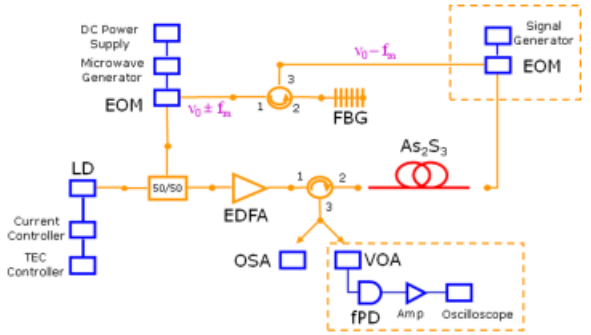

Fig. 14. Experimental setup used for gain and delay (dashed contour line) measurements. LD, laser diode; EOM, electro-optical modulator; FBG, fiber Bragg grating filter; EDFA, Er-doped fiber amplifier; VOA, variable optical attenuator; fPD, fast photodiode; Amp, electrical amplifier.

fiber due to its smaller core, lower loss, and slightly reduced refractive index.

A typical experimental setup for slow-light demonstration using chalcogenide fiber is detailed in Fig. 14. The components contained within the dashed contour lines were only used for the delay measurements. The output of a DFB laser (at 1548 nm) was split in two components, one that will serve as a pump while the other will serve as a counter-propagating signal. The signal component is frequency shifted by a certain amount (f_m) such as to match the Brillouin shift. Using a $LiNbO_3$ modulator and a signal generator, one can generate two side-bands, which are then separated by using a fiber Bragg grating (FBG) filter. The center frequency is suppressed through DC biasing. For the gain measurements, the signal is coupled into the chalcogenide fiber and the output is monitored with an OSA. For the delay measurements, the signal, before being coupled into the fiber, is modulated (sine wave at 25 MHz) with a $LiNbO_3$ modulator and a DS345 signal generator. The output is then passed through a variable optical attenuator (VOA) and detected with a fast photodiode and an amplifier on an oscilloscope. The VOA allowed us to control the signal on the detector such that we maintained the same signal (as low as possible) throughout the gain measurement to avoid any electronics-induced time response.

The pump is amplified with a standard Er-doped fiber amplifier and passed through a circulator before being coupled into the chalcogenide fiber, counter-propagating with the signal. The circulator allows us the signal to be picked off and sent to the detector.

The in-house drawn fiber used in this work was similar to the one used in previous work[33] but this time the fiber was cabled and both ends were antireflection coated. The fiber had a core of 5.2 μm diameter and a clad of 150 μm diameter, while the loss at 1550 nm was measured to be 0.138 m^{-1} (0.6 dB/m). The effective area of the fundamental mode was measured and the critical power, P_{th}, for a 10 m length of fiber was determined, directly from the variation, with pump power, of the counter-propagating signal generated through Brillouin scattering. This was performed in order to check the previous estimate of the g_B coefficient, which was obtained by rather qualitatively analyzing the spectral changes of signal.[33] By using A_{eff} and P_{cr} to determine g_B as detailed below, this approach follows the method used in previous work[28,37] although a more exact analysis was proposed elsewhere.[38]

The effective area (A_{eff}) was measured by imaging the fiber output on a vidicon camera using an appropriate microscope objective. A_{eff} was measured directly rather than using a theoretical estimate[28] due to the fact that the fiber had a very high NA (>0.30) making it possible for a second, higher order mode to contribute to the fundamental mode field. The measuring system was calibrated by also imaging a patch of SMF28 fiber with well-known MFD of 10.4 ± 0.8 μm at 1550 nm. The MFD for the chalcogenide fiber was thus determined to be 5.2 ± 0.4 μm.

The critical power was measured by monitoring the intensity of the Brillouin scattered signal versus the launched, counter-propagating pump power. A more precise analysis is usually performed in silica fibers.[35] The coupling efficiency was estimated from fiber throughput measurements. The reflected signal was collected using a circulator, and the values of the Brillouin peak were read directly from the OSA. Several measurements were made that yielded an average P_{th} of 29 ± 6 mW, which is close to the previously reported value of 27 ± 3 mW.[33] A typical data set is shown in Fig. 15.

Using Eq. (7), in which α is the fiber loss and L is the fiber length, an estimate of the effective fiber length (L_{eff}) can be obtained, giving a value of 5.4 m. Finally, one can use these values for A_{eff}, P_{th}, and L_{eff}, to estimate the Brillouin scattering coefficient using Eq. (5), where $k = 0.5$, in this case. Using proper error analysis, the Brillouin scattering coefficient was determined to be $(5.7 \pm 2.0) \times 10^{-9}$ m/W for the As_2S_3 fiber.

Additionally, the linewidth of the Brillouin signal was measured using a small probe (~ 8 μW) launched

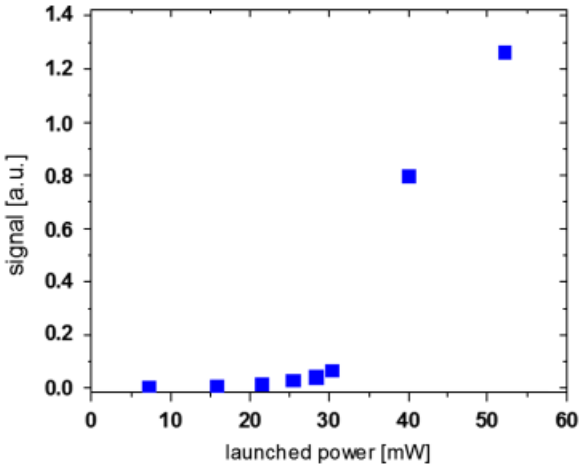

Fig. 15. Brillouin scattered signal in As_2S_3 fiber versus launched pump power.

counter-propagating through the fiber. The Brillouin shift was identified to be 7.96 GHz while the linewidth of the Brillouin shift was found to be 31 MHz with typical data being represented in Fig. 16. The linewidth was measured at low pump powers. Linewidth narrowing was observed for higher powers with linewidths as small as 19 MHz being recorded.

Gain and delay measurements using a small signal ($\sim$8 μW) have been performed in the chalcogenide fiber. For the gain measurement, the signal peak values were read from the OSA for different pump powers. For the delay measurement, the relative shift of the sine wave was read from the oscilloscope. A typical set of

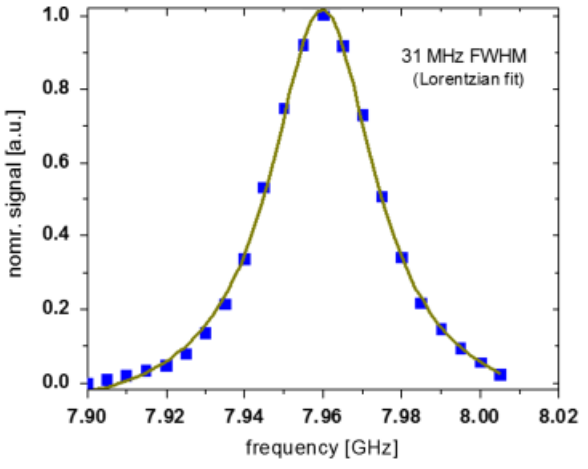

Fig. 16. Typical linewidth of the Brillouin signal at low pump power.

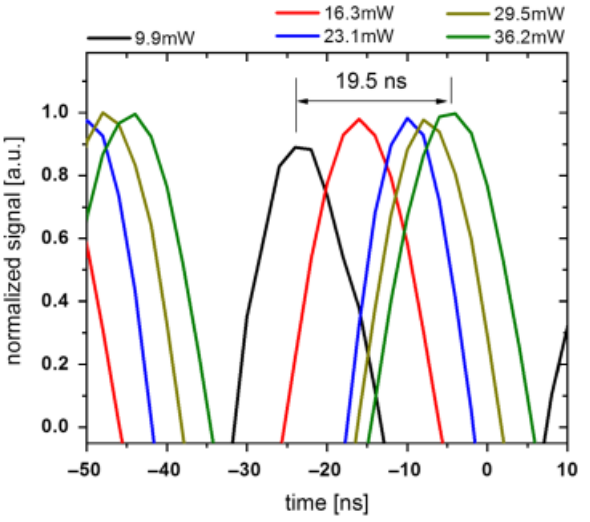

Fig. 17. Typical waveforms showing the delay for different pump powers.

traces is shown in Fig. 17. The observable gain and delay were limited by the damage threshold of the AR coating, which unfortunately was lower than the threshold for the bare As_2S_3 glass. A slow variation of the amplified signal was observed, which perhaps was due to the lack of polarization control in the setup. The overall results are represented in Fig. 18.

The slope of gain-versus-power is twice as large as the best previously reported result.[32] This was expected based on the analysis of the FOM for the SBS process in these fibers.[28,33] However, the gain slope falls short of the theoretical estimate. Using the undepleted pump approximation, the small-signal gain is given theoretically by the following equation:

$$G_{\text{th}}[\text{dB}] = 4.34\frac{g_B \times k \times L_{\text{eff}}}{A_{\text{eff}}} \times P \qquad (11)$$

Using the experimentally determined values for the appropriate parameters along with the associated uncertainties, Eq. (11) gives us a slope in the range (1.8–5.0) dB/mW. The inhomogenities in the fiber core diameter that we have noticed, the potential presence of a second mode, and the pump depletion approximation can be viewed as factors contributing to the discrepancy. The same factors can also influence the delay data. Once again, one can predict theoretically how much the peak of the signal pulse would be delayed (Δt) assuming an undepleted pump. The group velocity (given by $v_g = c/n_g$, c—speed of light, n_g total fiber group index) determines

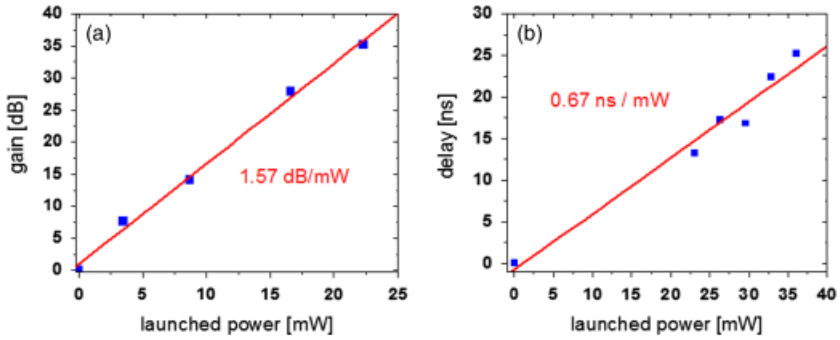

Fig. 18. (a) Gain and (b) pulse delay measurements in 10 m long As_2S_3 fiber at 1548 nm.

the time that a given pulse will take to travel the effective length of fiber. In the presence of the pump, the group velocity at the peak of the Brillouin gain will be modified according to the following equation, where $\Delta\upsilon$ is the linewidth (full-width half-maximum) of the Brillouin shift:[39]

$$\frac{1}{v_g} = \frac{n_{fg}}{c} + \frac{G/L_{eff}}{2\pi \times \Delta\nu} \tag{12}$$

For a narrow linewidth pulse the delay, that is the difference between the transit times required by the pulse with and without the pump, will then be given by the following equation:[39]

$$\Delta t \approx \frac{G}{2\pi \times \Delta\nu} = \frac{g_B \times k \times L_{eff}}{A_{eff} \times 2\pi \times \Delta\nu} \times P \tag{13}$$

Using the experimentally determined values for the parameters along with the associated uncertainties, Eq. (13) gives us a slope in the range [2.1–5.9] ns/mW. For this type of fiber, Eq. (13) indicates theoretically that delays on the order of 100 ns or more can be obtained for reasonable powers.

While in practical terms, a 19 ns delay was obtained for only 31 mW of pump power, which is marginally better than the result in the As_2Se_3 fiber,[32] these experimental values fall short of the theoretical expectations. The choice of the 25 MHz frequency for modulation of the signal was unfortunate because it turned out to be too close to the Brillouin linewidth, especially at low powers. In future work, we will try different modulation parameters and study the nature and origin of fiber imperfections and the role of polarization, which can negatively influence the performance of this system. This understanding will pave the way forward for delays of the order of 20 ns with as little as 10 mW of launched power.

Conclusions

The large nonlinearities and the fast response of the nonlinearity of the As–S–Se system make fibers drawn from these glasses well suited for optical switches and optical regenerators for high-speed telecommunication systems. Use of these materials will allow compact devices, cm's in length, with optical powers <1 W peak power (1 pJ in 1 ps pulses). The large Raman gain of the As–S–Se fibers coupled with the large IR transparency make these well suited for compact Raman amplifiers for telecommunications as well as fiber lasers and amplifiers in the mid-IR. These high nonlinearities also allow efficient supercontinuum generation, which is useful for broadband sources in the near and mid-IR.

The SBS process was studied in As_2S_3 and As_2Se_3 single-mode fibers. Values of the Brillouin gain coefficient were measured to be $(3.9 \pm 0.4) \times 10^{-9}$ m/W and $(6.75 \pm 0.35) \times 10^{-9}$ m/W, respectively. An analysis of the FOM for slow-light-based applications indicates that the smaller core As_2S_3 fiber performs best due to the lower loss, reduced core size, and slightly lower refractive index. The configuration using the small-core As_2S_3 fiber yields a FOM that is about 140 times larger, or a theoretical gain about 45 times larger, than the best silica-based configurations reported to date.

Finally these materials can be poled to induce an effective $\chi^{(2)}$, opening up the potential of waveguide parametric amplifiers. The continued improvement of chalcogenide materials will make such devices feasible in the near term.

References

1. Z. Borisova, "Glass Formation in Chalcogenide Systems and the Periodic System of Elements;" *Glassy Semiconductors*, 5–35, ed. Z. Borisova. Plennum Press, New York, NY, 1981.

2. J. Sanghera *et al.*, "Chalcogenide Optical Fibers Target Mid-IR Applications," *Laser Focus World*, 41 [4] 83–87 (2005).
3. J. Sanghera, L. Busse, and I. Aggarwal, "Effect of Scattering Centers on the Optical Loss of As_2S_3 Glass Fibers in the Infrared," *J. Appl. Phys.*, 75, 4885–4891 (1994).
4. J. Sanghera *et al.*, "Development of Low-Loss IR Transmitting Chalcogenide Glass Fibers," *SPIE*, 2396, 71–77 (1995).
5. J. Sanghera, V. Nguyen, P. Pureza, F. Kung, R. Miklos, and I. Aggarwal, "Fabrication of Low-Loss IR-Transmitting $Ge_{30}As_{10}Se_{30}Te_{30}$ Glass Fibers," *J. Lightwave Tech.*, 12, 737–741 (1994).
6. M. Churbanov, "Recent Advances in Preparation of High-Purity Chalcogenide Glasses in the USSR," *J. Non-Cryst. Solids*, 140, 324–330 (1992).
7. H. Nasu, Y. Ibara, and K. Kubodera, "Optical Third-Harmonic Generation from Some High-Index Glasses," *J. Non-Cryst. Solids*, 110, 229–234 (1989).
8. K. Richardson, J. McKinley, B. Lawrence, S. Joshi, and A. Villeneuve, "Comparison of Nonlinear Optical Properties of Sulfide Glasses in Bulk and Thin Film Form," *Opt. Mater.*, 10, 155–160 (1998).
9. G. Lenz *et al.*, "Large Kerr Effect in Bulk Se-Based Chalcogenide Glasses," *Opt. Lett.*, 25, 254–256 (2000).
10. J. Harbold *et al.*, "Highly Nonlinear As–S–Se Glasses for All-Optical Switching," *Opt. Lett.*, 27, 119–121 (2002).
11. R. Slusher, J. Hodelin, J. Sanghera, L. Shaw, and I. Aggarwal, "Large Raman Gain and Nonlinear Phase Shifts in High-Purity As_2Se_3 Chalcogenide Fibers," *JOSA-B*, 21, 1146–1155 (2004).
12. M. Asobe, H. Kobayashi, H. Itoh, and T. Kanamori, "Laser-Diode-Driven Ultrafast All-Optical Switching by Using Highly Nonlinear Chalcogenide Glass Fiber," *Opt. Lett.*, 18, 1056–1058 (1993).
13. M. Galili *et al.*, "Breakthrough Switching Speed with an All-Optical Chalcogenide Glass Chip:," *Opt. Express*, 17, 2182–2187 (2009).
14. M. Pelusi *et al.*, "Applications of Highly-Nonlinear Chalcogenide Glasss Devices Tailored for High-Speed All-Optical Signal Processing," *IEEE J. Sel. Top. Quant. Electron.*, 14, 529–539 (2008).
15. M. Asobe, T. Kanamori, K. Naganuma, H. Itoh, and T. Kaino, "Third-Order Nonlinear Spectroscopy in As_2S_3 Chalcogenide Glass Fibers," *J. Appl. Phys.*, 77, 5518–5523 (1995).
16. P. Thielen, L. Shaw, P. Pureza, V. Nguyen, J. Sanghera, and I. Aggarwal, "Small-Core As–Se Fiber for Raman Amplification," *Opt. Lett.*, 28, 1406–1408 (2003).
17. G. Devyatykh, M. Churbanov, I. Scripachev, E. Dianov, and V. Plotnichenko, "Middle Infrared As–S, As–Se, Ge–As–Se Chalcogenide Glass Fibers," *Int. J. Optoelectron.*, 7, 237–254 (1992).
18. S. Jackson and G. Anzueto-Sanchez, "Chalcogenide Glass Raman Fiber Laser," *Appl. Phys. Lett.*, 88, 221106-1–221106-3 (2006).
19. G. Edwards *et al.*, "Tissue Ablation by a Free-Electron Laser Tuned to the Amide II Band," *Nature*, 371, 416–418 (1994).
20. P. Thielen, L. Shaw, J. Sanghera, and I. Aggarwal, "Modeling of Mid-IR Chalcogenide Fiber Raman Laser," *Opt. Express*, 11, 3248–3253 (2003).
21. L. Shaw, P. Thielen, F. Kung, V. Nguyen, J. Sanghera, and I. Aggarwal, "IR Supercontinuum Generation in As–Se Photonic Crystal Fiber," *Proceedings of the Advanced Solid State Photonics Workshop*, TOPS, 98, Optical Society of America, 2005.
22. J. Hu, C. Menyuk, L. Shaw, J. Sanghera, and I. Aggarwal, "Raman Response Function and Supercontinuum Generation in Chalcogenide Fiber," *Proceedings of the Conference on Lasers and Electro-Optics (CLEO)*, Optical Society of America, 2008.
23. J. Hu, C. Menyuk, L. Shaw, J. Sanghera, and I. Aggarwal, "Generating Mid-IR Source Using As2S3-Based Chalcogenide Photonic Crystal Fibers," *Proceedings of the Conference on Lasers and Electro-Optics (CLEO)*, Optical Society of America, 2009.
24. E. Dianov, P. Kazansky, and D. Stepanov, "Problem of the Photoinduced Second Harmonic Generation in Optical Fibers," *Sov. J. Quant. Electron.*, 19, 575–576 (1989).
25. M. De Aruajo, M. Vermelho, A. Gouveia-Net, A. Sombra, and J. Medeiros Neto, "Efficient Second-Harmonic Generation in Praseodymium-Doped Ga:La:S Glass for 1.3 μm Optical Fiber Amplifiers," *IEEE Photon. Technol. Lett.*, 8, 821–823 (1996).
26. P. Kazansky, P. Russell, and H. Takabe, "Glass Fiber Poling and Applications," *J. Lightwave Tech.*, 15, 1484–1493 (1997).
27. A. Ruffin, "Stimulated Brillouin Scattering An Overview of Measurements, System Impairments, and Applications," *NIST Symposium on Optical Fiber Measurements*, Technical Digest, 23–28, 2004.
28. K. Song, K. Abedin, K. Hotate, M. Herráez, and L. Thévenaz, "Highly Efficient Brillouin Slow and Fast Light Using As_2Se_3 Chalcogenide Fiber," *Opt. Express*, 14, 5860–5865 (2006).
29. E. Ippen and R. Stolen, "Stimulated Brillouin Scattering in Optical Fibers," *Appl. Phys. Lett.*, 21, 539–541 (1972).
30. K. Ogusu, H. Li, and M. Kitao, "Brillouin-Gain Coefficients of Chalcogenide Glasses," *J. Opt. Soc. Am. B*, 21, 1302–1304 (2004).
31. C. Jáuregui, H. Ono, P. Petropoulos, and D. Richardson, "Four-Fold Reduction in the Speed of Light at Practical Power Levels Using Brillouin Scattering in a 2-m Bismuth-Oxide Fiber," OFC, Paper PDP2, 2006.
32. K. Abedin, G Lu, and T. Miyazaki, "Slow Light Generation in Singlemode Er-Doped Tellurite Fiber," *Electron. Lett.*, 44, 16–17 (2008).
33. C. Florea, M. Bashkansky, Z. Dutton, J. Sanghera, and I. Aggarwal, "Stimulated Brillouin Scattering in Single-Mode As_2S_3 and As_2Se_3 Chalcogenide Fibers," *Opt. Express*, 14, 12063–12070 (2006).
34. K. Song, M. Herráez, and L. Thévenaz, "Observation of Pulse Delaying and Advancement in Optical Fibers Using Stimulated Brillouin Scattering," *Opt. Express*, 13, 82–88 (2005).
35. A. Ruffin, M. Li, X. Chen, A. Kobyakov, and F. Annunziata, "Brillouin Gain Analysis for Fibers with Different Refractive Indices," *Opt. Lett.*, 30, 3123–3125 (2005).
36. J. Lee *et al.*, "Experimental Comparison of a Kerr Nonlinearity Figure of Merit Including the Stimulated Brillouin Scattering Threshold for State-of-the-Art Nonlinear Optical Fibers," *Opt. Lett.*, 30, 1698–1700 (2005).
37. K. Abedin, "Observation of Strong Stimulated Brillouin Scattering In Single-Mode As_2Se_3 Chalcogenide Fiber," *Opt. Express*, 13, 10266–10271 (2006).
38. K. Ogusu, "Analysis of Steady-State Cascaded Stimulated Brillouin Scattering in a Fiber Fabry–Pérot Resonator," *IEEE Photon. Tech. Lett.*, 14, 947–949 (2002).
39. Y. Okawachi *et al.*, "Tunable All-Optical Delays via Brillouin Slow Light in an Optical Fiber," *Phys. Rev. Lett.*, 94, 153902–153905 (2005).